DMD Fast Forward. Published on September 29, 2006 as doi:10.1124/dmd.106.009639

BIOTRANSFORMATION OF GELDANAMYCIN AND 17-ALLYLAMINO-17-DEMETHOXYGELDANAMYCIN BY HUMAN LIVER MICROSOMES: REDUCTIVE VERSUS OXIDATIVE METABOLISM AND IMPLICATIONS

Wensheng Lang, Gary W. Caldwell, Jian Li, Gregory C. Leo, William J. Jones, and John A. Masucci

Johnson and Johnson Pharmaceutical Research and Development, LLC, Spring House, Pennsylvania

Running title: IN VITRO METABOLISM OF GELDANAMYCIN AND 17AAG

Corresponding author: Wensheng Lang, Ph.D.
Johnson & Johnson Pharmaceutical Research and Development, LLC,
P.O. Box 776, Welsh and McKean Roads, Spring House, PA 19477

Telephone number: (215) 628-5960
Fax number: (215) 628-7064
E-mail address: wlang@prdus.jnj.com

28 text pages

5 tables

6 figures

34 references

213 words in Abstract

573 words in Introduction

1099 words in Discussion

Abbreviations: 17AAG, 17-allylamino-17-demethoxygeldanamycin; $GSGQH_2$, 19-glutathionyl geldanamycin hydroquinone; LC/QTOF-MS, liquid chromatography and quadrupole time of flight mass spectrometry; HLM, human liver microsomes; hP450R, human NADPH:cytochrome P450 reductase.

ABSTRACT:

Comparative metabolite profiling of geldanamycin and 17-allylamino-17-demethoxygeldanamycin (17AAG) using human liver microsomes in normoxia and hypoxia was conducted in order to understand their differential metabolic fates. Geldanamycin bearing a 17-methoxy group primarily underwent reductive metabolism, generating the corresponding hydroquinone under both conditions. The formed hydroquinone resists further metabolism and serves as a reservoir. Upon exposure to oxygen, this hydroquinone slowly reverts to geldanamycin. In the presence of glutathione, geldanamycin was rapidly converted to 19-glutathionyl-geldanamycin hydroquinone, suggesting its reactive nature. In contrast, the counterpart (17AAG) preferentially remained as its quinone form, which underwent extensive oxidative metabolism on both the 17-allylamino sidechain and the ansa ring. Only a small amount (<1%) of 19-glutathione conjugate of 17AAG was detected in the incubation of 17AAG with glutathione at 37^{o}C for 60 min. To confirm the differential nature of quinone-hydroquinone conversion between the two compounds, hypoxic incubations with human cytochrome P450 reductase at 37^{o}C and direct injection analysis were performed. Approximately 89% of hydroquinone, 5% of quinone, and 6% of 17-*O*-demethylgeldanamycin were observed after 1-min incubation of geldanamycin, whereas about 1% of hydroquinone and 99% of quinone were found in the 60-min incubation of 17AAG. The results provide direct evidence for understanding the 17-substituent effects of these benzoquinone ansamycins on their phase I metabolism, reactivity with glutathione and acute hepatotoxicity.

Introduction

The benzoquinone ansamycins geldanamycin and 17-allylamino-17-demethoxygeldanamycin (17AAG, Fig. 1) are potent antitumor agents that have undergone preclinical (Supko et al., 1995; Eiseman et al., 1997) and clinical (Banerji et al., 2005; Ramanathan et al., 2005) evaluations for their potential value in fighting cancers. The mechanism regarding the antineoplastic activity of these ansamycins has been extensively studied and showed to proceed through specific binding to the cytoplasmic heat shock protein-90 (HSP90) (Stebbins et al., 1997; Schulte and Neckers, 1998) and its endoplasmic reticulum homolog, glucose-regulated protein-94 (GRP94) (Chavany et al., 1996). Interaction of these ansamycins with the chaperone protein folding machinery results in disruption of heteroprotein complexes and blocking of the refolding and conformational maturation of numerous oncogenic client proteins, i.e., $p185^{erbB2}$ (Miller et al., 1994; Schnur et al., 1995), HER2 (Basso et al., 2000), $pp60^{v\text{-}src}$ (Whitesell et al., 1994), Raf-1 (Stancato et al., 1997), mutant p53 (An et al., 1997), and HIF-1 (Mabjeesh et al., 2002), which are involved in signal transduction in regulation of cell proliferation, apoptosis and angiogenesis. It is known that the unfolded client proteins are susceptible to degradation via the ubiquitination-proteasome pathway. However, recent findings from electron spin resonance studies of the production of reactive oxygen species (i.e., superoxide anion and hydrogen peroxide) mediated by geldanamycin leading to oxidative stress and cell death argued against the HSP90 inhibition theory (Benchekroun et al., 1994; Dikalov et al., 2002; Billecke et al., 2002). In general, quinone drugs are biotransformed into the corresponding semiquinone radicals upon reductive activation by NADPH:cytochrome P450 reductase or microsomal fraction (Bachur et al.,1978; Kalyanaraman et al., 1980). The subsequent disproportionation of the semiquinone radicals results in the formation of the corresponding hydroquinones and quinones. On exposure to

oxygen, these semiquinones can be oxidized into the parent quinones together with superoxide anion being released. The dismutation of superoxide anion leads to the formation of hydrogen peroxide and molecular oxygen. The formed hydroquinones can also be oxidized to the parent quinones by molecular oxygen directly, but slowly. Thus far, the potential quinone-hydroquinone interconversion of geldanamycin has not been assessed although several *in vitro* and *in vivo* metabolism studies of 17AAG have been published (Egorin et al., 1998; Musser et al., 2003, Guo et al., 2005). In addition, emerging evidence has demonstrated the higher binding affinity of a benzohydroquinone to HSP90 than its corresponding quinone (Shen and Blagg, 2005; Guo et al., 2005). We think that geldanamycin may share the same feature and potentially be more cytotoxic to hypoxic solid tumors compared to the normal oxygenated tissues upon bioreductive activation. Therefore, conducting a comparative study on the quinone-hydroquinone conversion of the two ansamycins upon metabolic activation is important in order to understand their differences in HSP90-mediated cytotoxicity, pharmacokinetics, and hepatotoxicity.

In this study, we monitored the metabolite profiles of these ansamycins after incubations with human liver microsomes and human NADPH:cytochrome P450 reductase in normoxia and hypoxia using liquid chromatography and quadrupole time-of-flight mass spectrometry. Particularly, we have focused on the quinone-hydroquinone conversion. The metabolites in incubations were characterized by LC/QTOF-MS/MS, UV-Vis and accurate mass measurement. The relative percentages of the components in incubations were estimated using a normalization method based on the integrated peak areas of composite-ion chromatograms. On the basis of the identified metabolite profiles, the biotransformation pathways for each ansamycin in human liver microsomes were proposed. The possible mechanism leading to the differential metabolism between the two ansamycins is discussed.

Materials and Methods

Materials. Geldanamycin, 17AAG, glutathione reduced form, glucose-6-phosphate disodium salt, β-nicotinamide adenine dinucleotide phosphate sodium salt (β-NADP-Na), glucose-6-phosphate dehydrogenase, sodium dihydrogenphosphate monohydrate, magnesium chloride hexahydrate, deuterium oxide and formic acid (guarantee grade) were purchased from Sigma-Aldrich (St. Louis, MO). Sodium phosphate dibasic heptahydrate was obtained from J.T. Baker (Phillisburg, NJ). Acetonitrile and water (HPLC grade) were purchased from EMD Chemicals (Gibbstown, NJ). Pooled human liver microsomes (20 mg protein/ml) and recombinant human NADPH:cytochrome P450 reductase (hP450R, 2.4 mg/ml) were obtained from BD Biosciences (Worburn, MA). The specific activity of hP450R was 41 μmol cytochrome c reduced per min per mg of protein. The specific activity of P450R in human liver microsomes was 400 nmol reduced cytochrome c per min per mg of protein.

Incubation with HLM. Incubations of geldanamycin and 17AAG with pooled human liver microsomes in the presence of an NADPH regenerating system with or without 5 mM glutathione in normoxia and hypoxia at 37^{o}C were conducted as previously described (Lang et al., 2005). Briefly, 0.10 M sodium phosphate buffer solution (2.0 ml, pH 7.4) containing 1 mM β-NADP, 5 mM glucose-6-phosphate and 5 mM magnesium chloride was transferred into a vial. A 1 unit/μl glucose-6-phosphate dehydrogenase solution (5 μl) and the appropriate amount of 20 mg/ml pooled human liver microsomes were added into the vial. The mixture was pre-incubated at 37^{o}C for 3 min, and then 2.5 mM compound stock solution (8 μl) was added to initiate the enzymatic reaction. An aliquot of 400 μl of the incubation mixture was transferred into a 1.5-ml microcentrifuge tube containing 800 μl of acetonitrile at 1, 15, 30 and 60 min. The sample was

mixed on a vortex mixer, and then was centrifuged at 7,200g for 5 min at room temperature. The supernatant (500 μl) was transferred into a 2-ml HPLC vial containing 1000 μl of water for LC/QTOF-MS and LC/QTOF-MS/MS analyses. To evaluate reactivity with glutathione, incubations of the compounds with 5 mM glutathione in 0.1 M sodium phosphate buffer solution (pH 7.4) in the absence of HLM at 37^{o}C were also conducted. In hypoxic incubation, a 0.10 M potassium phosphate buffer solution (2.0 ml, pH 7.4) containing 1 mM β-NADP, 5 mM glucose-6-phosphate, 5 mM magnesium chloride and 10 μM geldanamycin or 17AAG was pre-incubated and bubbled with 100% helium gas (the tip of the helium gas supply was submerged approximately 2 mm in the solution) for 3 min. HLM (100 μl) were added and mixed. The tip of the helium gas supply was then moved approximately 1 mm above the surface of the incubation fluid. The enzymatic reaction proceeded under the positive pressure of helium gas during the course of incubation at 37^{o}C. The rest of the procedures for sample preparation and analysis are the same as described above. In addition, incubations of the test compounds with HLM in 0.10 M sodium phosphate buffer solution (pH 7.4) in the absence of NADP and glutathione were conducted as negative controls under both aerobic and anaerobic conditions.

Incubation with hP450R. Incubations of geldanamycin and 17AAG with human NADPH:cytochrome P450 reductase at equivalent activity (1 μl of 41 μmole/mg/min P450R solution) were conducted at 37^{o}C under normoxic and hypoxic conditions. One volume of the incubation fluid was mixed with 2 volumes of acetonitrile at 1, 30 and 60 min for protein precipitation prior to LC/QTOF-MS analysis as described above. For direct injection analysis, the incubation fluid (5 μl) was injected directly onto the LC/QTOF-MS system at 1, 30 and 60 min.

LC-DAD-MS. An Agilent 1100 series LC system (Agilent Technologies, Palo Alto, CA), consisting of a quaternary pump, a degasser, an autosampler and a diode array detector (DAD), was used for this study. Separation of metabolites was carried out on a Zobarx SB-C18 column (2.1 × 150 mm, 3.5 μm, Agilent). Mobile phases A, 0.1% formic acid in water, and B, 0.08% formic acid in water-acetonitrile (10:90), were used for a linear gradient elution as follows: 20-80% B in 20 min, hold 80% B for 5 min, return to 20% B in 0.1 min, post run time of 6 min. DAD wavelength range was 210-700 nm with a 2 nm interval. The flow rate was set at 0.20 ml/min and the sample injection volume was 5 μl. For hydrogen/deuterium exchange LC-MS analysis, the mobile phases were prepared with deuterated water and the other HPLC conditions remained the same as above. A Micromass quadrupole orthogonal acceleration time-of-flight *Ultima Global* mass spectrophotometer (Waters, Milford, MA) was interfaced with the LC system through a Z-spray electrospray ionization source and was operated in the positive ion mode. This instrument was equipped with a lock spray, a 4.0-GHz time-to-digital converter and a reflectron, which generated a resolving power of 9300 at m/z 556.2771 (FWHM definition for leucine enkephalin). MassLynx 4.0 software was used for system control and data processing. Nitrogen was used as nebulizing gas, desolvation gas and cone curtain gas. Argon was chosen as collision gas with the collision cell gas pressure at 10 psi. The QTOF-MS source parameters were set as follows: capillary voltage, 3000 V; cone voltage, 40 V; source temperature, 120^{o}C; desolvation temperature, 250^{o}C; cone gas flow, 100 L/h; and desolvation gas flow, 500 L/h. The microchannel plates (MCP) detector was operated at 2100 V. An m/z range of 100-950 was recorded in every 1.0 s with an interscan time of 0.10 s for QTOF-MS analysis. These parameters remained the same as above except for the collision energy of 15-17 eV for QTOF-

MS/MS analysis. For accurate mass measurement, a 0.1 μM leucine enkephalin solution was infused into the lock spray at 5 μl/min to provide a lock mass of m/z 556.2771.

Molecular Modeling. Schrödinger MacroModel-eMBrAcE module (New York, NY) was applied to energy minimization and interaction energy calculation for geldanamycin hydroquinone-HSP90 and quinone-HSP90 complexes. The x-ray crystal structure of geldanamycin-HSP90 complex (PDB code: 1yet) (Stebbins et al., 1997) was used as a starting point for energy optimization. The bond orders of co-crystallized geldanamycin were corrected and all water molecules were removed. The hydrogen atoms were added to the protein structure and the ionizable residues and salt bridges were treated using the standard protein preparation procedure in Schrödinger Maestro 7.5 (New York, NY). During the calculation, OPLS-AA force-field (Jorgensen et al., 1996) and GB/SA continuum water model (Qui et al., 1997) were used. Protein residues within 8 Å of the binding site were allowed to optimize and all other residues were held fixed. Similar to the co-crystal structure, geldanamycin hydroquinone and quinone in the optimized complexes adopted a cis amide conformation. The calculated MacroModel-eMBrAcE interaction energies for geldanamycin hydroquinone- and quinone-HSP90 complexes and the key hydrogen bond distances were summarized for comparison.

Characterization of Metabolites. The characterization of metabolites is primarily based on LC/QTOF-MS/MS analysis. The metabolites were assigned by comparing retention time and MS/MS fragmentation with the corresponding parent compound. Additionally, accurate mass measurement of the metabolites was conducted in order to confirm their elemental composition. The on-line scan UV-Vis absorption spectra of the metabolites were used for differentiation between quinone and hydroquinone forms.

17AAG hydroquinone (M1). M1 had a retention time of 10.52 min and a protonated molecular ion at m/z 588 (parent + 2). The MS/MS spectrum of M1 showed a series of product ions at m/z 527 $(MH - HOCONH_2)^+$, 495 $(MH - HOCONH_2 - CH_3OH)^+$, 477 $(MH - HOCONH_2 - CH_3OH - H_2O)^+$, 463 $(MH - HOCONH_2 - 2CH_3OH)^+$, 454 (base peak, $MH - HOCONH_2 - CH_2{=}CH\text{-}CH{=}NH - H_2O)^+$, 445 $(MH - HOCONH_2 - 2CH_3OH - H_2O)$, 436 $(MH - HOCONH_2 - CH_2{=}CH\text{-}CH{=}NH - 2H_2O)$, 422 $(MH - HOCONH_2 - CH_2{=}CH\text{-}CH{=}NH - CH_3OH - H_2O)$, 404 $(MH - HOCONH_2 - CH_2{=}CH\text{-}CH{=}NH - CH_3OH - 2H_2O)$, 291, 260, 242, 204, 187 ($C_{1\text{-}10}$, $^+CO\text{-}C(CH_3){=}CH\text{-}CH{=}CH\text{-}C\Xi C\text{-}C(CH_3){=}CH\text{-}CH_2CH_3$), 173, 159 (187 - CO), 133 and 107. The UV-Vis spectrum of 17AAG hydroquinone showed characteristic absorption bands at 238, 258 and 310 nm (sh). Accurate mass of M1 calculated for $C_{31}H_{46}N_3O_8$ $(M + H)^+$: 588.3285; found: 588.3270.

6-O-Demethyl-17-(2',3'-dihydroxypropylamino)-geldanamycin (M2). M2 had a retention time of 11.20 min and a protonated molecular ion at m/z 606 (parent – 14 + 16 + 18). The MS/MS spectrum of M2 showed a series of product ions at m/z 588 $(MH - H_2O)^+$, 545 $(MH - HOCONH_2)^+$, 527 (base peak, $MH - HOCONH_2 - H_2O)^+$, 513 $(MH - HOCONH_2 - CH_3OH)^+$, 495 $(MH - HOCONH_2 - CH_3OH - H_2O)^+$, 419, 324, 187 ($C_{1\text{-}10}$, $^+CO\text{-}C(CH_3){=}CH\text{-}CH{=}CH\text{-}C\Xi C\text{-}C(CH_3){=}CH\text{-}CH_2CH_3$) and 159 $(187 - CO)^+$. The UV-Vis spectrum of M2 showed absorption bands at 222, 250 (sh), 334 and 532 nm. Accurate mass of M2 calculated for $C_{30}H_{44}N_3O_{10}$ $(M + H)^+$: 606.3027; found: 606.3008.

12-O-Demethyl-17-(2',3'-dihydroxypropylamino)-geldanamycin (M3). M3 had a retention time of 12.11 min and a protonated molecular ion at m/z 606 (parent – 14 + 16 + 18). The MS/MS spectrum of M3 showed product ions at m/z 574 $(MH - CH_3OH)^+$, 545 $(MH - HOCONH_2)^+$, 513 (base peak, $MH - HOCONH_2 - CH_3OH)^+$, 495 $(MH - HOCONH_2 - CH_3OH -$

$H_2O)^+$, 422, 394, 327, 187 and 159. The UV-Vis spectrum of M3 showed absorption bands at 222, 250 (sh), 334 and 532 nm. Accurate mass of M3 calculated for $C_{30}H_{44}N_3O_{10}$ $(M + H)^+$: 606.3027; found: 606.3054.

22-Hydroxyl-17-(2',3'-dihydroxypropylamino)-geldanamycin (M4). M4 had a retention time of 12.51 min and a protonated molecular ion at m/z 636 (parent + 16 + 18 +16). The MS/MS spectrum of M4 showed a series of product ions at m/z 604 $(MH - CH_3OH)^+$, 575 $(MH - HOCONH_2)^+$, 543 (base peak, $MH - HOCONH_2 - CH_3OH)^+$, 525 $(MH - HOCONH_2 - CH_3OH - H_2O)^+$, 511 $(MH - HOCONH_2 - 2CH_3OH)^+$, 420, 367, 323, 203 ($C_{1\text{-}10}$, $^+$CO-C(CH_2OH)=CH-CH=CH-CΞC-C(CH_3)=CH-CH_2CH_3), 175 ($C_{2\text{-}10}$, $^+$C(CH_2OH)=CH-CH=CH-CΞC-C(CH_3)=CH-CH_2CH_3), 149 and 125. The UV-Vis spectrum of M4 showed absorption bands at 222, 250 (sh), 334 and 532 nm. Accurate mass of M4 calculated for $C_{31}H_{46}N_3O_{11}$ $(M + H)^+$: 636.3132; found: 636.3130.

17-(2',3'-Dihydroxypropylamino)-geldanamycin (M5). M5 had a retention time of 13.66 min and a protonated molecular ion at m/z 620 (parent + 16 + 18). The MS/MS spectrum of M5 showed a series of product ions at m/z 588 $(MH - CH_3OH)^+$, 559 $(MH - HOCONH_2)^+$, 527 (base peak, $MH - HOCONH_2 - CH_3OH)^+$, 509 $(MH - HOCONH_2 - CH_3OH - H_2O)^+$, 495 $(MH - HOCONH_2 - 2CH_3OH)^+$, 477 $(MH - HOCONH_2 - 2CH_3OH - H_2O)^+$, 324, 219 ($C_{1\text{-}10}$, $^+$CO-C(CH_3)=CH-CH=CH-C(OCH_3)=CH-C(CH_3)=CH-CH_2CH_3) and 187 ($C_{1\text{-}10}$, $^+$CO-C(CH_3)=CH-CH=CH-CΞC-C(CH_3)=CH-CH_2CH_3). The UV-Vis spectrum of M5 showed absorption bands at 222, 250 (sh), 334 and 532 nm. Accurate mass of M5 calculated for $C_{31}H_{46}N_3O_{10}$ $(M + H)^+$: 620.3183; found: 620.3158.

17-(Didehydroallylamino)-geldanamycin (M6). M6 had a retention time of 13.99 min and a protonated molecular ion at m/z 584 (parent – 2). The MS/MS spectrum of M6 showed a series

of product ions at m/z 523 $(MH - HOCONH_2)^+$, 491 (base peak, $MH - HOCONH_2 - MeOH)^+$, 473 $(MH - HOCONH_2 - CH_3OH - H_2O)^+$, 459 $(MH - HOCONH_2 - 2CH_3OH)^+$, 441 $(MH - HOCONH_2 - 2CH_3OH - H_2O)^+$, 351, 305, 217, 187 ($C_{1\text{-}10}$, $^+CO\text{-}C(CH_3)=CH\text{-}CH=CH\text{-}C\Xi C\text{-}C(CH_3)=CH\text{-}CH_2CH_3$) and 160. The UV-Vis spectrum of M6 showed absorption bands at 222, 250 and 532 nm. Accurate mass of M6 calculated for $C_{31}H_{42}N_3O_8$ $(M + H)^+$: 584.2972; found: 584.2963.

17-(3'-Hydroxyallylamino)-geldanamycin (M7). M7 had a retention time of 14.34 min and a protonated molecular ion at m/z 602 (parent + 16). The MS/MS spectrum of M7 showed a series of product ions at m/z 541 $(MH - HOCONH_2)^+$, 509 $(MH - CH_3OH - HOCONH_2)^+$, 491 $(MH - CH_3OH - HOCONH_2 - H_2O)^+$, 477 $(MH - 2CH_3OH - HOCONH_2)^+$, 459 $(MH - 2CH_3OH - HOCONH_2 - H_2O)^+$**,** 449, 415, 365, 261, 187 ($C_{1\text{-}10}$, $^+CO\text{-}C(CH_3)=CH\text{-}CH=CH\text{-}C\Xi C\text{-}C(CH_3)=CH\text{-}CH_2CH_3$) and 159 $(187 - CO)^+$. Accurate mass of M7 calculated for $C_{31}H_{44}N_3O_9$ $(M + H)^+$: 602.3078; found: 602.3052.

17-Aminogeldanamycin (M8). M8 had a retention time of 15.96 min. The full scan mass spectrum of M8 showed two strong molecular adduct ions at m/z 563 $(M + NH_4)^+$ and 568 $(M + Na)^+$ and a minor protonated molecular ion at m/z 546 (parent – 40). The MS/MS spectrum of M8 acquired from the ammonium adduct ion showed a series of product ions at m/z 514 $(MH - NH_3 - CH_3OH)^+$, 485 $(MH - NH_3 - HOCONH_2)^+$, 453 (base peak, $MH - NH_3 - CH_3OH - HOCONH_2)^+$, 435 $(MH - NH_3 - CH_3OH - HOCONH_2 - H_2O)^+$, 421 $(MH - NH_3 - 2CH_3OH - HOCONH_2)^+$, 403 $(435.2 - CH_3OH/\ 421.2 - H_2O)^+$, 219 ($C_{1\text{-}10}$, $^+CO\text{-}C(CH_3)=CH\text{-}CH=CH\text{-}C(OCH_3)=CH\text{-}C(CH_3)=CH\text{-}CH_2CH_3$) and 187 ($C_{1\text{-}10}$, $^+CO\text{-}C(CH_3)=CH\text{-}CH=CH\text{-}C\Xi C\text{-}C(CH_3)=CH\text{-}CH_2CH_3$). The UV-Vis spectrum of M8 showed maximum absorption peaks at

242, 328 and 532 nm. Accurate mass of M8 calculated for $C_{28}H_{43}N_4O_8$ $(M + NH_4)^+$: 563.3081; found: 563.3074.

12-O-Demethyl-17AAG (M9). M9 had a retention time of 16.52 min and a protonated molecular ion at m/z 572 (parent – 14). The MS/MS spectrum of M9 showed a series of product ions at m/z 540 $(MH - CH_3OH)^+$, 511 $(MH - HOCONH_2)^+$, 479 (base peak, $MH - HOCONH_2 - CH_3OH)^+$, 461 $(MH - HOCONH_2 - CH_3OH - H_2O)^+$, 443 $(MH - HOCONH_2 - CH_3OH - 2H_2O)^+$, 293, and 187 ($C_{1\text{-}10}$, $^+CO\text{-}C(CH_3)=CH\text{-}CH=CH\text{-}C\Xi C\text{-}C(CH_3)=CH\text{-}CH_2CH_3$). The UV-Vis spectrum of M9 showed maximum absorption bands at 242, 334 and 532 nm. Accurate mass of M9 calculated for $C_{30}H_{42}N_3O_8$ $(M + H)^+$: 572.2972; found: 572.2936.

22-Hydroxyl-17AAG (M10). M10 had a retention time of 18.08 min and a protonated molecular ion at m/z 602 (parent + 16). The MS/MS spectrum of M10 showed a series of product ions at m/z 570 $(MH - CH_3OH)^+$, 541 $(MH - HOCONH_2)^+$, 509 (base peak, $MH - CH_3OH - HOCONH_2)^+$, 491 $(MH - CH_3OH - HOCONH_2 - H_2O)^+$, 460, 386, 203 ($C_{1\text{-}10}$, $^+CO\text{-}C(CH_2OH)=CH\text{-}CH=CH\text{-}C\Xi C\text{-}C(CH_3)=CH\text{-}CH_2CH_3$), 175 $(203.1 - CO)^+$ and 125. The UV-Vis spectrum of M10 showed absorption bands at 242, 334 and 532 nm. Accurate mass of M10 calculated for $C_{31}H_{44}N_3O_9$ $(M + H)^+$: 602.3078; found: 602.3060.

17AAG. 17AAG had a retention time of 20.00 min. The full scan mass spectrum of 17AAG showed a cluster of molecular ions at m/z 586 $(M + H)^+$, 603 $(M + NH_4)^+$ and 608 $(M + Na)^+$ together with the in-source fragment ions at m/z 554 $(MH - CH_3OH)^+$, 525 $(MH - HOCONH_2)^+$ and 493 (base peak, $MH - HOCONH_2 - CH_3OH)^+$. The MS/MS spectrum of 17AAG acquired from the protonated molecular ion showed a series of product ions at m/z 525 $(MH - HOCONH_2)^+$, 493 (base peak, $MH - HOCONH_2 - CH_3OH)^+$, 475 $(MH - HOCONH_2 - CH_3OH - H_2O)^+$, 461 $(MH - HOCONH_2 - 2CH_3OH)^+$, 443 $(MH - HOCONH_2 - 2CH_3OH - H_2O)^+$, 385, 187

(C_{1-10}, $^{+}CO\text{-}C(CH_3)=CH\text{-}CH=CH\text{-}C\Xi C\text{-}C(CH_3)=CH\text{-}CH_2CH_3$), 159 (187 - CO) and 107. The UV-Vis spectrum of 17AAG showed maximum absorption peaks at 242, 334 and 532 nm. Accurate mass of 17AAG calculated for $C_{31}H_{44}N_3O_8$ $(M + H)^+$: 586.3128; found: 586.3128.

Geldanamycin. Geldanamycin had a retention time of 18.78 min. The full scan mass spectrum of geldanamycin showed a strong sodium adduct at m/z 583 $(M + Na)^+$ and lack of the protonated molecular ion at m/z 561. A series of in-source fragment ions at m/z 500 $(MH - HOCONH_2,)^+$, 468 $(MH - CH_3OH - HOCONH_2)^+$, 450 $(MH - CH_3OH - HOCONH_2 - H_2O)^+$, 436 $(MH - 2CH_3OH - HOCONH_2)^+$ and 418 $(MH - 2CH_3OH - HOCONH_2 - H_2O)^+$ were observed. The UV-Vis spectrum of geldanamycin showed absorption bands at 260, 304 nm and 430 nm (sh). Accurate mass of geldanamycin calculated for $C_{29}H_{40}N_2O_9Na$ $(M + Na)^+$: 583.2632; found: 583.2628.

Geldanamycin hydroquinone. Geldanamycin hydroquinone had a retention time of 11.46 min. The full scan mass spectrum of geldanamycin showed a cluster molecular ions at m/z 563 $(M + H)^+$, 580 $(M + NH_4)^+$ and 585 $(M + Na)^+$ and a series of in-source fragment ions at m/z 531, $(MH - CH_3OH)^+$, 502 $(MH - HOCONH_2,)^+$, 470 $(MH - CH_3OH - HOCONH_2)^+$ and 438 $(MH - 2CH_3OH - HOCONH_2)^+$. The UV-Vis spectrum showed characteristic absorption bands at 250 and 298 nm (sh). Accurate mass of geldanamycin hydroquinone calculated for $C_{29}H_{43}N_2O_9$ $(M + H)^+$: 563.2969; found: 563. 2957.

17-O-Demethylgeldanamycin (17DMG). 17DMG had a retention time of 16.37 min and a strong sodium adduct ion at m/z 569. The MS/MS spectrum of 17DMG acquired from the sodium adduct ion showed a series of product ions at m/z 508 $(MNa - HOCONH_2)^+$, 476 $(MNa - HOCONH_2 - CH_3OH)^+$, 458 $(MNa - HOCONH_2 - CH_3OH - H_2O)^+$, 444 $(MNa - HOCONH_2 - 2CH_3OH)^+$, 369**,** 187 ($C_{1-10}$, $^{+}CO\text{-}C(CH_3)=CH\text{-}CH=CH\text{-}C\Xi C\text{-}C(CH_3)=CH\text{-}CH_2CH_3$), 174, 159

(187 - CO)$^+$, 131, and 107. The UV-Vis spectrum of 17DMG showed absorption bands at 246, 310 and 532 nm. Accurate mass of 17DMG calculated for $C_{28}H_{38}N_2O_9Na$ $(M + Na)^+$: 569.2475; found: 569. 2484.

19-Glutathionyl-geldanamycin hydroquinone (GSGQH$_2$). $GSGQH_2$ had a retention time of 8.22 min and a protonated molecular ion at m/z 868 (parent + 307). The MS/MS spectrum of $GSGQH_2$ showed a series of product ions at m/z 807 $(MH - HOCONH_2)^+$, 775.3 (base peak, MH - $HOCONH_2$ - $CH_3OH)^+$, 757 (MH - $HOCONH_2$ - CH_3OH - $H_2O)^+$, 743 (MH - $HOCONH_2$ - $2CH_3OH)^+$, 700 (775 - glycine)$^+$, 646 [775 - 129 (dehydrated glutamic acid, a diagnostic fragment of glutathione conjugation)], 187 (C_{1-10}, $^+$CO-C(CH_3)=CH-CH=CH-CΞC-C(CH_3)=CH-CH_2CH_3) and 159 (187 - CO)$^+$. The UV-Vis spectrum of $GSGQH_2$ showed absorption bands at 258 and 310 (sh) nm. Accurate mass of $GSGQH_2$ calculated for $C_{39}H_{58}N_5O_{15}S$ $(M + H)^+$: 868.3650; found: 868.3699.

Results

Relative Percentages of Metabolites in Incubations. The relative percentages of geldanamycin and its metabolites in incubations with HLM and hP450R at various incubation times are given in Table 1. The results indicated that geldanamycin was highly metabolized by HLM, generating the corresponding hydroquinone (73%) at 60 min in both normoxia and hypoxia. A quicker onset of the reductive metabolism in hypoxia was obtained within 1 min, suggesting oxygen exposure may play a role in attenuation of the rate of the reductive reaction. A minor product, 17-*O*-demethylgeldanamycin, was observed in the incubations. This product was also found in the incubation of geldanamycin with a 0.1 M sodium phosphate buffer solution (pH 7.4) in the absence of any metabolizing enzymes (data not shown). The finding suggests that 17-*O*-demethylgeldanamycin may be a degradation product of geldanamycin in the aqueous

medium. No significant amount of oxidative metabolites of geldanamycin in the incubations with HLM was detected.

In order to evaluate the role of hP450R in the reductive metabolism of geldanamycin, separate incubations of geldanamycin with hP450R were conducted under both conditions. Approximately 80% of geldanamycin hydroquinone and 16% of geldanamycin were obtained in the normoxic incubation at 60 min, and the similar results were found in the hypoxic incubation at the same time (Table 1). To minimize the oxygen exposure during sample preparation after incubation, we used direct injection analysis of the hypoxic hP450R incubation samples. Approximately 89% of geldanamycin hydroquinone was observed after 1-min incubation (Table 2). In contrast, only about 1% of hydroquinone was found in the hypoxic incubation of 17AAG with hP450R at 60 min (Fig. 2). Further follow-up analyses of the incubations revealed that the formed hydroquinones slowly reverted to the corresponding parent quinones upon exposure to oxygen (data not shown).

In the presence of glutathione, geldanamycin was mainly metabolized into 19-glutathionyl-geldanamycin hydroquinone ($GSGQH_2$, 70%) and geldanamycin hydroquinone (GQH_2, 23%) in the normoxic incubation with HLM at 60 min (Table 3). In addition, approximately 2% of 19-glutathionyl-geldanamycin quinone (GSGDM) and 4% of 17-*O*-demethylgeldanamycin (17DMG) were detected over the course of incubation. The structures of these metabolites and the proposed biotransformation pathways for geldanamycin in HLM in the presence of NADPH and glutathione are given in Fig. 3. These products were also found in the control incubation with 5 mM glutathione in the absence of HLM (Table 3). The relative content was 67% for $GSGQH_2$, 17% for GSGDM, 8% for 17DMG, and 2% for GQH_2 at 60 min. The spontaneous

reaction of geldanamycin with glutathione may be an indication associated with its high toxicity (Cysyk et al. 2006)

The relative percentages of the identified components in incubations of 17AAG with HLM in normoxia are presented in Table 4. It was found that 17AAG was completely metabolized after 30 min of incubation with HLM at 1 mg/ml protein. In order to elucidate the biotransformation pathways for 17AAG, incubation of 17AAG with the reduced amount of HLM at 0.2 mg/ml protein was conducted. Approximately 2% of 17AAG hydroquinone (M1) and about 47% of 17AAG quinone was found in this incubation at 60 min. In the presence of glutathione, similar metabolite profile of 17AAG in HLM was observed in comparison with that obtained without this trapping agent. No significant amount of glutathione conjugate of 17AAG was detected in the incubation.

Identification of Metabolites. Identification of metabolites was conducted using LC-QTOF MS/MS, UV Vis and accurate mass measurement. The UV-Vis absorption spectra of the metabolites proved very useful to distinguish between quinones and hydroquinones (Fig. 4). A total of ten metabolites of 17AAG were observed and tentatively identified in the incubation with HLM at 0.2 mg/ml protein. Of these, M1 was the only hydroquinone metabolite with a remarkably different UV/Vis spectrum (λ_{max} 238, 258 and 310 nm) from that of 17AAG. The full scan mass spectrum of M1 showed a predominant protonated molecular ion at m/z 588 (parent + 2). The MS/MS spectrum of M1 showed several unique fragment ions at m/z 454, 436, 422 and 404, associated with the loss of the allylamino sidechain. M1 was assigned as 17AAG hydroquinone.

M2 and M3 had the identical protonated molecular ion at m/z 606 (parent + 16 + 18 – 14), suggesting the isomers may be from oxidation, hydration and *O*-demethylation. The metabolites

had different MS/MS fragmentation patterns with a base peak at m/z 527 for M2 and 513 for M3. These base peaks may correspond to the loss of carbamic acid and water, and carbamic acid and methanol, respectively, from the protonated molecular ion. Therefore, the position of *O*-demethylation was tentatively assigned at the C6 for M2 and the C12 for M3. M5 was the most abundant metabolite in HLM incubations. This metabolite has a protonated molecular ion at m/z 620 (parent + 16 +18), consistent with oxidation and hydration of 17AAG (Fig. 5). M5 was assigned as a diol metabolite. M6, M8 and M9 are three metabolites with a protonated molecular mass less than 17AAG by 2, 40 and 14 a.m.u, respectively. The amount of M6 in the incubations with HLM increased with time (Table 4), indicating this product is relatively stable. M6 is believed to be generated from dehydration of α-hydroxylated 17AAG on the allylamino sidechain (Fig. 5). The observation of a mass shift of 5 a.m.u. for the protonated molecular ion of M6 in H/D exchange LC/MS analysis supports the structure assignment. M8 was a major metabolite of 17AAG with a protonated molecular ion at m/z 546 (parent – 40), consistent with the loss of the allyl sidechain from the parent. The UV/Vis spectrum and MS/MS fragmentation pattern of M8 were similar to those of 17AAG. M8 was assigned as 17-aminogeldanamycin. M9 had a protonated molecular ion at m/z 572 (parent - 14), consistent with demethylation. The observation of the predominant MS/MS fragment ion at m/z 479, corresponding to the loss of methanol and carbamic acid from the protonated molecular ion of M9, indicates that demethylation may occur at the C12 position. M10 had a protonated molecular ion at m/z 602 (parent +16), consistent with monooxydation. The observation of a characteristic MS/MS fragment ion at m/z 203 suggests that the oxydation may occur in the $C_{1\text{-}10}$ region of 17AAG. M10 was tentatively assigned as 22-hydroxyl-17AAG.

Discussion

The metabolite profile of geldanamycin obtained from the hypoxic incubation with hP450R via direct injection analysis indicates that this compound was rapidly reduced to the corresponding hydroquinone (~89%) after 1 min (Table 2). A less amount (78%) of the hydroquinone was obtained from a separate hypoxic incubation with hP450R at 60 min using a protein precipitation procedure. These results indicate that oxygen exposure during sample preparation may cause some of the hydroquinone oxidized into the parent quinone. However, a comparable amount (80%) of the hydroquinone was observed in the normoxic incubation with hP450R at 60 min using the same protein precipitation procedure. The findings suggest the rate of formation of geldanamycin hydroquinone catalyzed by hP450R is much faster than that of oxidation of the hydroquinone to quinone by molecular oxygen. Therefore, the reactions proceed in favor of the hydroquinone formation in the normoxic incubation with hP450R. The relative amount of geldanamycin hydroquinone in the final stage (60 min) of the normoxic or hypoxic incubation mainly depends on the hP450R activity. Similar metabolite profiles of geldanamycin were obtained from the incubations with HLM, which had an equivalent hP450R activity (Table 1). Surprisingly, no oxidative metabolites of geldanamycin in the normoxic incubations with HLM were observed.

In contrast, a much smaller amount (~1%) of hydroquinone was obtained from the hypoxic incubation of 17AAG with hP450R via direct injection analysis. The results imply that 17AAG preferentially remains as its quinone form in the presence of the one-electron reduction enzyme (hP450R). Although the quinone-to-hydroquinone conversion of 17AAG catalyzed by a two-electron reduction enzyme DT-diaphorase has previously been reported (Guo et al., 2005), the two enzymes have different redox potentials and work through different mechanisms.

DMD Fast Forward. Published on September 29, 2006 as DOI: 10.1124/dmd.106.009639
This article has not been copyedited and formatted. The final version may differ from this version.

The difference in hP450R mediated quinone-hydroquinone conversion between the two 17-substituted analogs is associated with their redox potentials relative to that of hP450R. A single-electron redox potential of –0.283 V for hP450R in a phosphate buffer solution (pH 7.0) has been reported (Munro et al., 2001). The one-electron redox potentials of the benzoquinone ansamycins can be predicted using the Hammett equation (Wardman, 1990):

$$\Delta E = E_{subQ} - E_Q = Q\sum\sigma_{para}$$

where ΔE is the difference between the one-electron redox potentials of substituted and unsubstituted quinones, E_Q is the one-electron redox potential of an unsubstituted quinone (i.e., +0.080 V for parabenzoquinone in water), Q is a constant for a specific type of quinone (i.e., 0.61 V for parabenzoquinone in water), and σ_{para} is the Hammett para substituent constant. The ΔE value for geldanamycin was estimated to be –0.323 V based on the σ_{para} values of –0.27, –0.26, and 0.00 for the substituents of -OCH_3, -CH_2CH_2-, and -$NHCOCH_3$, respectively. Thus, the one-electron redox potential of geldanamycin (E_{GDM}) in water was calculated to be –0.243 V. A lower redox potential for 17AAG was calculated to be –0.390 V based on the σ_{para} values of –0.51, –0.26 and 0.00 for the substituents of -$NHCH_2CH_2$, -CH_2CH_2- and -$NHCOCH_3$, respectively. The σ_{para} values used for these calculations were obtained either from the same substituent or the similar substituent listed in the literature (Hansch et al., 1991). The calculated redox potentials for geldanamycin and 17AAG support our findings that geldanamycin is easily reduced by hP450R, but 17AAG is not. The 17-allylamino group of 17AAG is a stronger electron-donating substituent than the 17-methoxy of geldanamycin. Therefore, this functionality is responsible for a more negative shift in one-electron redox potential for 17AAG. As a result, 17AAG is not as easily reduced by hP450R as compared to geldanamycin.

The results of metabolite identification indicate that the biotransformation of geldanamycin by HLM differs from that of 17AAG. Reductive metabolism and nucleophilic addition on the benzoquinone ring are two major biotransformation pathways for geldanamycin, while the extensive oxidative metabolism of 17AAG on both the 17-allylamino side chain and the ansa ring is predominant. The data suggest that geldanamycin benzoquinone may serve as a strong electrophile in CYP heme-quinone complex. Following a one-electron reduction, the heme-quinone complex may undergo an internal electron transfer, generating a ferric-semiquinone complex Fe^{3+}-[$Q^{\cdot-}$]. The second one-electron reduction followed by the subsequent internal electron transfer of the ferrous-semiquinone complex produces a ferric-hydroquinone complex Fe^{3+}-[QH_2]. The further one-electron reduction and molecular oxygen binding to the ferrous-hydroquinone complex lead to the formation of a tris ferrous-dioxygen-hydroquinone complex. In this reaction cycle, the formed ferric-hydroperoxo-hydroquinone complex is unstable and quickly dissociates to Fe^{3+}-[Q] and H_2O before generating the activated iron-oxene (Fe=O) complex. It has been known that the iron-oxene formation is a key step in the oxidative metabolism. Understanding the non-productive reaction cycle of geldanamycin leading to the resistance against the oxidative metabolism is important in general. The resistance against oxidative metabolism for other quinone anticancer agents (i.e., porfiromycin and mitomycin C) has been observed previously (Lang et al., 2000; Lang et al., 2005). For 17AAG, the internal electron transfer from ferrous-quinone complex Fe^{2+}-[Q] to ferric-semiquinone complex Fe^{3+}-[$Q^{\cdot-}$] may not proceed efficiently. Dioxygen-binding to the ferrous-quinone complex is then activated and forms the iron-oxene-quinone complex, which turns over to various oxidative products.

In order to assess the interactions of hydroquinone and quinone binding to HSP90 protein, we carried out a molecular modeling calculation on geldanamycin hydroquinone-HSP90 and quinone-HSP90 complexes (Table 5). Our results show that geldanamycin hydroquinone binding to HSP90 is more energetically favored as compared to its quinone form, which is consistent with the recent findings for radester (Shen and Blaggs, 2005) and 17AAG (Guo et al., 2005). Analysis of the hydrogen-bonding pattern in geldanamycin hydroquinone-HSP90 complex can provide insight into understanding this interaction energy calculation result. As shown in Fig.6, two more hydrogen bonds are formed between the hydroxyl groups of geldanamycin hydroquinone and the sidechain of Asn51, and the carbonyl oxygen of Gly135 backbone in the GQH_2-HSP90 complex. These two hydrogen bonds do not exist in its quinone-HSP90 complex. The data suggest that the quinone-hydroquinone conversion associated with the functional switch of geldanamycin from hydrogen bond acceptors to hydrogen bond donors leads to a tighter binding to HSP90. The results imply the potential preferential cytotoxicity of geldanamycin to the hypoxic solid tumors compared to the normal oxygenated tissues.

In conclusion, the comparative metabolite profiling using human liver microsomes in normoxia and hypoxia reveals the selective reductive metabolism of geldanamycin and oxidative metabolism of 17AAG, respectively. The extensive oxidative metabolism of 17AAG occurs primarily on the 17-allylamino sidechain. The conversion of geldanamycin quinone into the hydroquinone in the presence of hP450R may result in a higher binding affinity to HSP90. The reactive nature of geldanamycin toward the cellular scavenger glutathione is an indication correlated with its high hepatic toxicity. The findings provide a foundation for discovery of metabolically stable and less toxic geldanamycin analogs targeted to the hypoxic solid tumors.

Acknowledgements. We thank Dr. Keith T. Demarest for critical review of this manuscript and Dr. Robert A. Galemmo, Jr. for helpful discussions.

References

An WG, Schnur RC and Neckers L (1997) Depletion of $p185^{erbB2}$, Raf-1 and mutant p53 proteins by gledanamycin derivatives correlates with antiproliferative activity. *Cancer Chemother Pharmacol* 40:60-64.

Bachur NR, Gordon SL and Gee MV (1978) A general mechanism for microsomal activation of quinone anticancer agents to free radicals. *Cancer Res* 38:1745-1750.

Banerji U, O'Donnell A, Scurr M, Pacey S, Stapleton S, Asad Y, Simmons L, Maloney A, Raynaud F, Campbell M, Walton M, Lakhani S, Kaye S, Workman P and Judson I (2005) Phase I pharmacokinetic and pharmacodynamic study of 17-allylamino, 17-demethoxy-geldanamycin in patients with advanced malignancies. *J Clin Oncol* 23:4152-4161.

Basso AD, Solit DB, Munster PN and Rosen N (2000) Ansamycin antibiotics inhibit Akt activation and cyclin D expression in breast cancer cells that overexpress HER2. *Oncogen* 21:1159-1166.

Benchekroun MN, Myers CE and Sinha BK (1994) Free radical formation by ansamycin benzoquinone in human breast tumor cells: Implications for cytotoxicity and resistance. *Free Radical Bio Med* 17:191-200.

Billecke SS, Bender AT, Kanelakis KC, Murphy PJM, Lowe ER, Kamada Y, Pratt WB and Osawa Y (2002) Hsp90 is required for heme binding and activation of apo-neuronal nitric-oxide synthase: Geldanamycin-mediated oxidant generation is unrelated to any action of hsp90. *J Biol Chem* 277:20504-20509.

Chavany C, Mimnaught E, Miller P, Bitton R, Nguyent P, Trepel J, Whitesell L, Schnur R, Moyer JD and Neckers L (1996) $p185^{erbB2}$ binds to GRP94 in vivo: Dissociation of the

p185^{erbB2}/GRP94 heterocomplex by benzoquinone ansamycins proceeds depletion of p185^{erbB2}. *J Biol Chem* 271:4974-4977.

Cysyk RL, Parker RJ, Barchi JJ, Steeg PS, Hartman NR and Strong JM (2006) Reaction of geldanamycin and C17-substituted analogues with glutathione: Product identifications and pharmacological implications. *Chem Res Toxicol* 19:376-381.

Dikalov S, Landmesser U and Harrison DG (2002) Geldanamycin leads to superoxide formation by enzymatic and non-enzymatic redox cycling: Implications for studies of HSP90 and endothelial cell nitric-oxide synthase. *J Biol Chem* 277:25480-25485.

Egorin MJ, Rosen DM, Wolff JH, Callery PS, Musser SM and Eiseman JL (1998) Metabolism of 17-(allylamino)-17-demethoxygeldanamycin (NSC 330507) by murine and human hepatic preparations. *Cancer Res* 58:2385-2396.

Eiseman JL, Sentz DL, Zuhowski EG, Ramsland TS, Rosen, DM, Reyna SP and Egorin MJ (1997) Plasma pharmacokinetics and tissue distribution of 17-allylaminogeldanamycin, a prodrug for geldanamycin in CD2F$_1$ mice and Fisher 344rats. *Proc Am Assoc Cancer Res* 38:308.

Guo W, Reigan P, Siegel D, Zirrolli J, Gustafson D and Ross D (2005) Formation of 17-allylamino-demethoxygeldanamycin (17-AAG) hydroquinone by NAD(P)H:quinone oxidoreductase 1: Role of 17-AAG hydroquinone in heat shock protein 90 inhibition. *Cancer Res* 65:10006-10015.

Hansch C, Leo A and Taft RW (1991) A survey of Hammett substituent constants and resonance and field parameters. *Chem Rev* 91:165-195.

Jorgensen WL, Maxwell DS and Tirado-Rives J (1996) Development and testing of the OPLS all-atom force field on conformational energies and properties of organic liquids. *J Am Chem Soc* 118: 11225-11236.

Kalyanaraman B, Perez-Reyes E and Mason RP (1980) Spin-trapping and direct electron spin resonance investigations of the redox metabolism of quinone anticancer drugs. *Biochim Biophy Acta* 630:119-130.

Lang W, Caldwell GW and Masucci JA (2005) Evaluation of the effect of oxygen exposure on human liver microsomal metabolism of mitomycin C in the presence of glutathione using liquid chromatography–quadrupole time of fight mass spectrometry. *Anal Biochem* 343:268-276.

Lang W, Mao J, Doyle TW and Almassian B (2000) Isolation and identification of urinary metabolites of porfiromycin in dogs and humans. *Drug Metab Dispos* 28:899-904.

Lang W, Mao J, Wang Q, Niu C, Doyle TW and Almassian B (2000) Isolation and identification of metabolites of porfiromycin formed in a rat liver preparation. *J Pharm Sci* 89:191-198.

Mabjeesh NJ, Post DE, Willard MT, Kaur B, Van Meir, EG, Simons JW and Zhong H (2002) Geldanamycin induces degradation of hypoxia-inducible factor 1α protein via the proteosome pathway in prostate cancer cells. *Cancer Res* 62:2478-2482.

Maroney AC, Marugan JJ, Mezzasalma TM, Barnakov AN, Garrabrant TA, Weaner LE, Jones WJ, Barnakova LA, Koblish HK, Todd MJ, Masucci JA, Deckman IC, Galemmo RA and Johnson DL (2006) Dihydroquinone ansamycins: Towards resolving the conflict between low in vitro affinity and high cellular potency of geldanamycin derivatives. *Biochemistry* 45:5678-5685.

Miller P, DiOrio C, Moyer M, Schnur RC, Bruskin A, Cullen W and Moyer JD (1994) Depletion of the erbB-2 gene product p185 by benzoquinonoid ansamycins. *Cancer Res* 54:2724-2730.

Munro AW, Noble MA, Robledo L, Daff SN and Chapman SK (2001) Determination of the redox properties of human NADPH-cytochrome P450 reductase. *Biochemistry* 40:1956-1963.

Musser SM, Egorin MJ, Zuhowski EG, Hamburger DR, Parise RA, Covey JM, White KD and Eiseman JL (2003) Biliary excretion of 17-(allylamino)-17-demethoxygeldanamycin (NSC 330507) and metabolites by Fischer 344 rats. *Cancer Chemother Pharmacol* 52:139-46.

Qui D, Shenkin PS, Hollinger FP and Still CW (1997) The GB/SA continuum model for salvation. A first analytic method for the calculation of approximate Born radii. *J Phys Chem A* 101: 3005-3014.

Ramanathan RK, Trump DL, Eiseman JL, Belani CP, Agarwala SS, Zuhowski EG, Lan J, Potter DM, Ivy SP, Ramalingam S, Brufsky AM, Wong MK, Tutchko S and Egorin MJ (2005) Phase I pharmacokinetic-pharmacodynamic study of 17-(allylamino)-17-demethoxygeldanamycin (17AAG, NSC 330507), a novel inhibitor of heat shock protein 90, in patients with refractory advanced cancers. *Clin Cancer Res* 11:3385-3391.

Schnur RC, Corman ML, Gallaschun RJ, Cooper BA, Dee MF, Doty JL, Muzzi ML, Moyer JD, DiOrio CI, Barbacci EG, Miller PE, O'Brien AT, Morin MJ, Foster BA, Pollack VA, Savage DM, Sloan DE, Pustilnik LR and Moyer MP (1995) Geldanamycin and dihydrogeldanamycin derivatives. *J Med Chem* 38:3806-3812.

Schnur RC, Corman ML, Gallaschun RJ, Cooper BA, Dee MF, Doty JL, Mumi ML, DiOrio CI, Barbacci EG, Miller PE, Pollack VA, Savage DM, Sloan DE, Pustilnik LR, Moyer JD and

Moyer MP (1995) *erbB-2* Oncogene inhibition by geldanamycin derivatives: synthesis, mechanism of action, and structure-activity relationships. *J Med Chem* 38:3813-3820.

Schulte TW and Neckers LM (1998) The benzoquinone ansamycin 17-allyamino-17-demethoxygeldanamycin binds to HSP90 and shares important biologic activities with geldanamycin. *Cancer Chemother Pharmacol* 42:273-279.

Shen G and Blagg BSJ (2005) Radester, a novel inhibitor of the Hsp90 protein folding machinery. *Organic Letters* 7:2157-2160.

Stancato LF, Silverstein AM, Owens-Grillo JK, Chow Y, Jove R and Pratt WB (1997) The hsp90-binding antibiotic geldanamycin decreases Raf levels and epidermal growth factor signaling without disrupting formation of signaling complexes or reducing the specific enzymatic activity of Raf kinase. *J Biol Chem* 272:4013-4020.

Stebbins CE, Russo AA, Schneider C, Rosen N, Hartl FU and Pavletich NP (1997) Crystal structure of an Hsp90–geldanamycin complex: targeting of a protein chaperone by an antitumor agent. *Cell* 89:239–250.

Supko JG, Hickman RL, Grever MR and Malspeis L (1995) Preclinical pharmacologic evaluation of geldanamycin as an antitumor agent. *Cancer Chemother Pharmacol* 36:305-315.

Wardman P (1990) Bioreductive activation of quinones: Redox properties and thiol reactivity. *Free Rad Res Comms* 8:219-229.

Whitesell L, Mimnaugh EG, De Costat B, Myers CE and Neckers LM (1994) Inhibition of heat shock protein HSP90-pp60$^{v\text{-}src}$ heteroprotein complex formation by benzoquinone ansamycins: Essential role for stress proteins in oncogenic transformation. *Proc Natl Acad Sci USA* 91:8324-8328.

Legends for figures

Fig. 1. Structures of geldanamycin (GDM) and 17-allylamino-17-demethoxygeldanamycin (17AAG).

Fig. 2. Composite-ion chromatograms of geldanamycin (GDM) and 17AAG incubations with hP450R in hypoxia at 60 min via direct injection analysis. 17AAGQH_2, 17AAG hydroquinone; GQH_2, geldanamycin hydroquinone; 17-DMG, 17-*O*-demethylgeldanamycin.

Fig. 3. Biotransformation pathways of geldanamycin in human liver microsomes in the presence of NADPH and glutathione.

Fig. 4. UV-Vis absorption spectra of geldananmycin (GDM), geldanamycin hydroquinone (GQH_2) and 19-glutathionyl-geldanamycin hydroquinone (GSGQH_2).

Fig. 5. Oxidative biotransformation pathways of 17-allylamino-17-demethoxygeldanamycin in human liver microsomes in the presence of an NADPH regenerating system.

Fig. 6. Binding interactions of geldanamycin hydroquinone with HSP90.

DMD Fast Forward. Published on September 29, 2006 as DOI: 10.1124/dmd.106.009639
This article has not been copyedited and formatted. The final version may differ from this version.

TABLE 1

Relative percentages of identified components in incubations of geldanamycin with human liver microsomes (1.0 mg/ml protein) and human NADPH:cytochrome P450 reductase (hP450R) under normoxic and hypoxic conditions

	Time	Normoxia			Hypoxia		
	(min)	GDM	GQH_2	17DMG	GDM	GQH_2	17DMG
HLM	1	59	40	<1	25	74	<1
	30	31	68	<1	29	71	<1
	60	26	73	<1	26	73	<1
hP450R	1	90	6	4	39	56	5
	30	18	78	4	21	74	5
	60	16	80	4	18	78	4

Values are expressed as normalized signal area intensity of geldanamycin and major metabolites. GDM, geldanamycin; GQH_2, geldanamycin hydroquinone; 17DMG, 17-*O*-demethylgeldanamycin.

DMD Fast Forward. Published on September 29, 2006 as DOI: 10.1124/dmd.106.009639
This article has not been copyedited and formatted. The final version may differ from this version.

TABLE 2

Relative percentages of identified components in incubations of geldanamycin and 17AAG with human NADPH:cytochrome P450 reductase in hypoxia via direct injection analysis

Time (min)	GDM	GDM GQH_2	17AAG	17AAG	17AAGQH_2
1	5	89	6	99	<1
30	4	90	6	99	1
60	5	89	6	99	1

GDM, geldanamycin; GQH_2, geldanamycin hydroquinone; 17DMG 17-*O*-demethylgeldanamycin, 17AAG, 17-allylamino-17-demethoxygeldanamycin; 17AAGQH_2, 17-allylamino-17-demethoxygeldanamycin hydroquinone.

DMD Fast Forward. Published on September 29, 2006 as DOI: 10.1124/dmd.106.009639
This article has not been copyedited and formatted. The final version may differ from this version.

TABLE 3

Relative percentages of identified components in incubations of geldanamycin with 5 mM glutathione in the presence or absence of human liver microsomes (1 mg/ml protein) in normoxia

	Time (min)	GDM	$GSGQH_2$	GSGDM	GQH_2	17DMG
GSH + HLM	1	17	54	2	22	5
	15	3	64	2	26	5
	30	2	68	2	24	4
	60	1	70	2	23	4
GSH	1	27	55	6	5	6
	15	4	77	9	4	6
	60	6	67	17	2	8

Values are expressed as normalized signal area intensity of geldanamycin and major metabolites. GDM, geldanamycin; GQH_2, geldanamycin hydroquinone; $GSGQH_2$, 19-glutathionyl-geldanamycin hydroquinone; GSGDM, 19-glutathionyl-geldanamycin; 17DMG, 17-*O*-demethylgeldanamycin.

TABLE 4

Relative percentages of identified components in incubations of 17AAG with human liver microsomes in normoxia at 37°C

HLM	Time (min)	17AAG	M1	M2	M3	M4	M5	M6	M7	M8	M9	M10
0.2 mg/ml protein	1	97.4	1.4	0.0	0.0	0.0	0.0	0.4	0.3	0.3	0.0	0.2
	15	79.6	2.1	0.1	0.3	0.8	8.4	1.9	0.6	4.7	0.8	0.8
	30	66.5	2.8	0.2	0.5	1.6	14.9	2.5	1.0	7.7	1.0	1.3
	60	47.0	2.0	0.3	0.9	2.6	24.8	3.6	1.8	13.4	1.1	2.2
1.0 mg/ml protein	1	92.7	1.3	0.1	0.0	0.2	1.9	1.9	0.0	1.8	0.0	0.0
	30	0.0	0.0	0.9	4.9	9.8	52.5	6.1	0.0	25.8	0.0	0.0
	60	0.0	0.0	2.6	6.6	12.3	51.0	7.7	0.0	19.9	0.0	0.0
GSH[a]	1	89.2	1.6	0.0	0.0	0.3	4.5	1.9	0.0	2.4	0.0	0.0
	30	0.0	0.0	1.5	4.7	9.9	50.3	8.7	0.0	25.0	0.0	0.0
	60	0.0	0.0	2.5	7.9	10.0	47.3	11.1	0.0	21.1	0.0	0.0

[a]Incubation with HLM (1.0 mg/ml protein) in the presence of 5 mM glutathione

DMD Fast Forward. Published on September 29, 2006 as DOI: 10.1124/dmd.106.009639
This article has not been copyedited and formatted. The final version may differ from this version.

TABLE 5

Interaction energy (kcal/mol) between HSP90 and geldanamycin quinone/hydroquinone

Ligand	E_{vdw}	E_{ele}	E_{sol}	E_{total}	H-Bond Distance (Å)[a]	
Hydroquinone	-57.3	-68.2	18.5	-107.0	Gly135: hydroquinone O-H	1.93
					Lys112: hydroquinone H··O	1.82
					Asn51: hydroquinone O-H	2.10
Quinone	-58.1	-61.4	21.0	-98.5	Lys112: quinone C=O	2.40

[a] Only H-bonds formed by quinone/hydroquinone group are shown. E_{total}, total interaction energy; E_{vdw}, van der Waals; E_{ele}, electrostatic energy; $E_{sol,}$ salvation.

DMD Fast Forward. Published on September 29, 2006 as DOI: 10.1124/dmd.106.009639
This article has not been copyedited and formatted. The final version may differ from this version.

Fig. 1

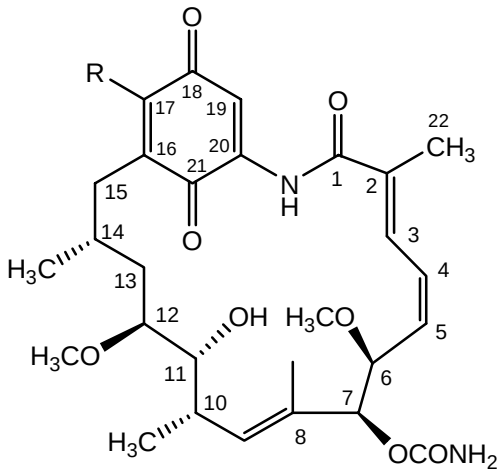

R = OCH_3, **GDM**

R = $NHCH_2CH{=}CH_2$, **17AAG**

DMD Fast Forward. Published on September 29, 2006 as DOI: 10.1124/dmd.106.009639
This article has not been copyedited and formatted. The final version may differ from this version.

Fig. 2

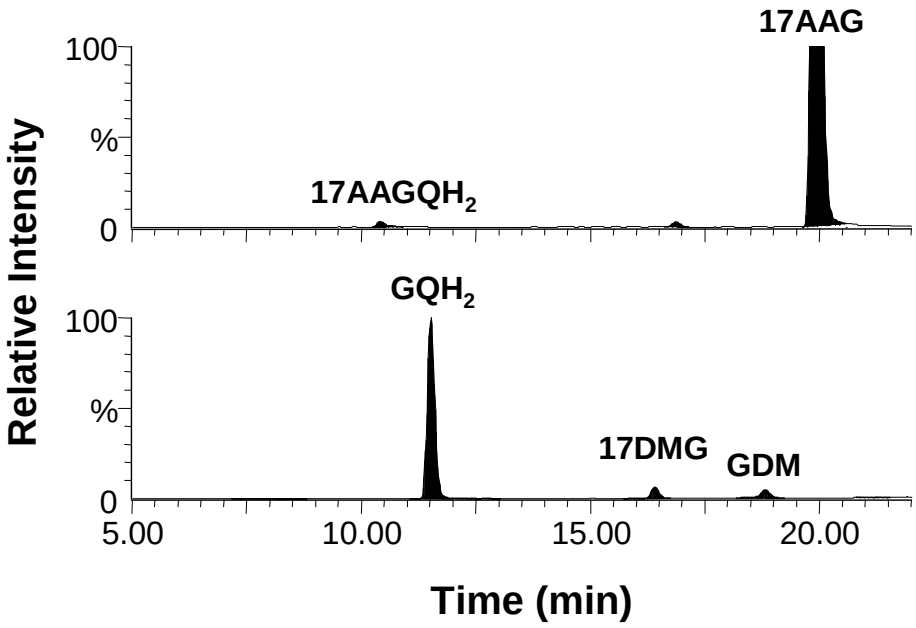

DMD Fast Forward. Published on September 29, 2006 as DOI: 10.1124/dmd.106.009639
This article has not been copyedited and formatted. The final version may differ from this version.

Fig. 3

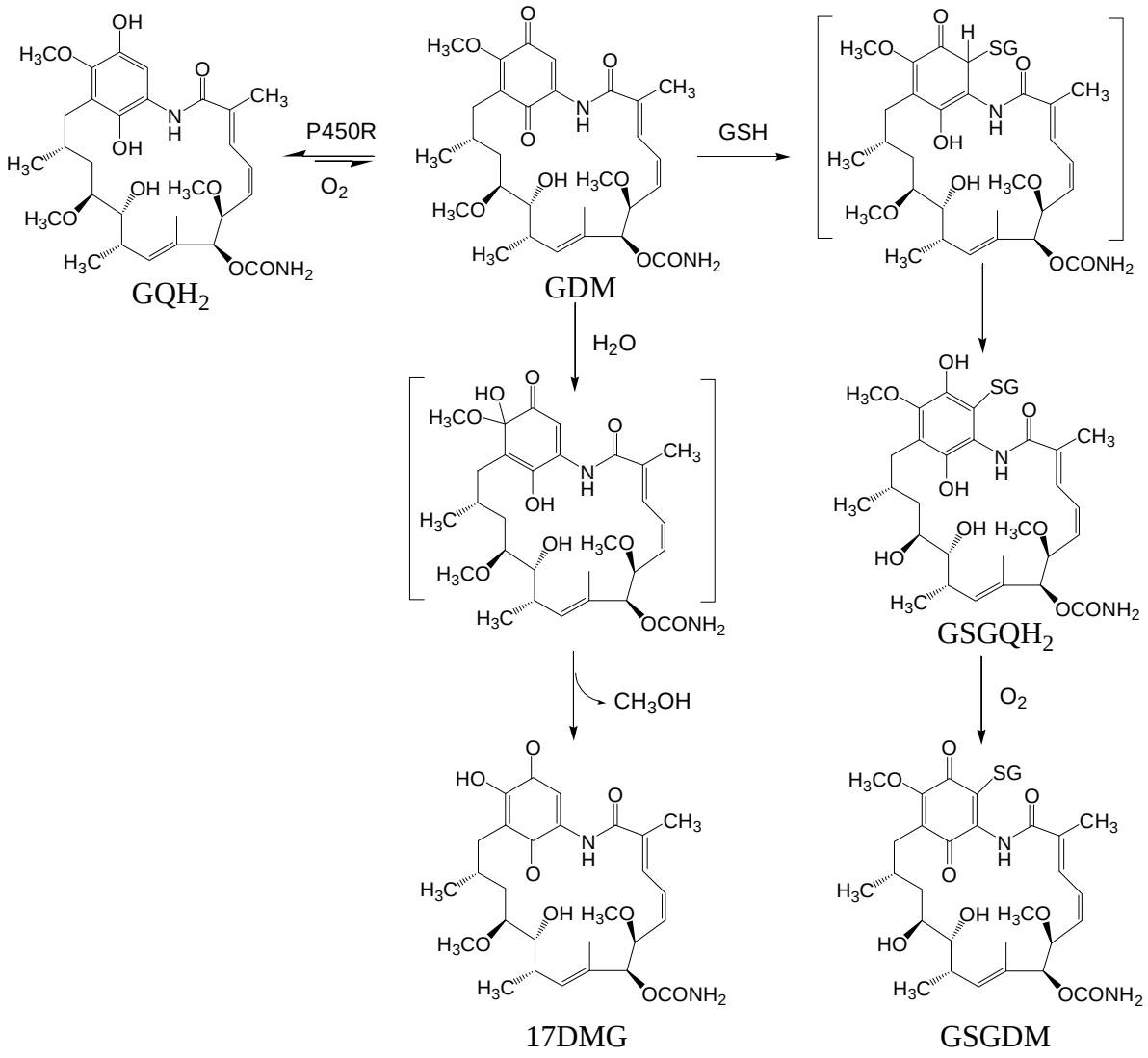

DMD Fast Forward. Published on September 29, 2006 as DOI: 10.1124/dmd.106.009639
This article has not been copyedited and formatted. The final version may differ from this version.

Fig. 4

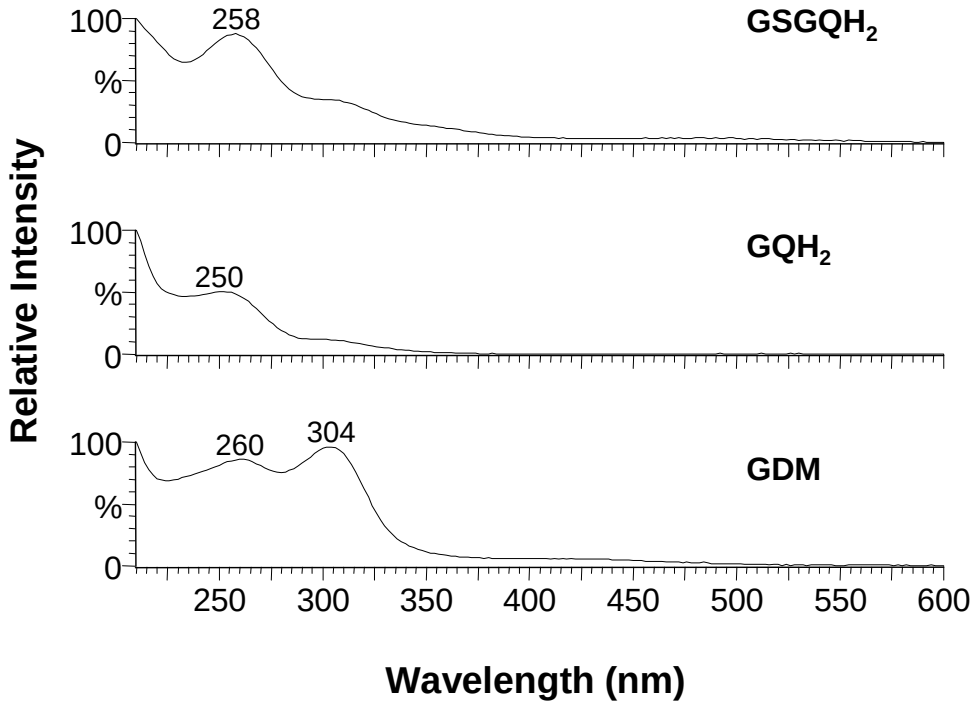

DMD Fast Forward. Published on September 29, 2006 as DOI: 10.1124/dmd.106.009639
This article has not been copyedited and formatted. The final version may differ from this version.

Fig. 5

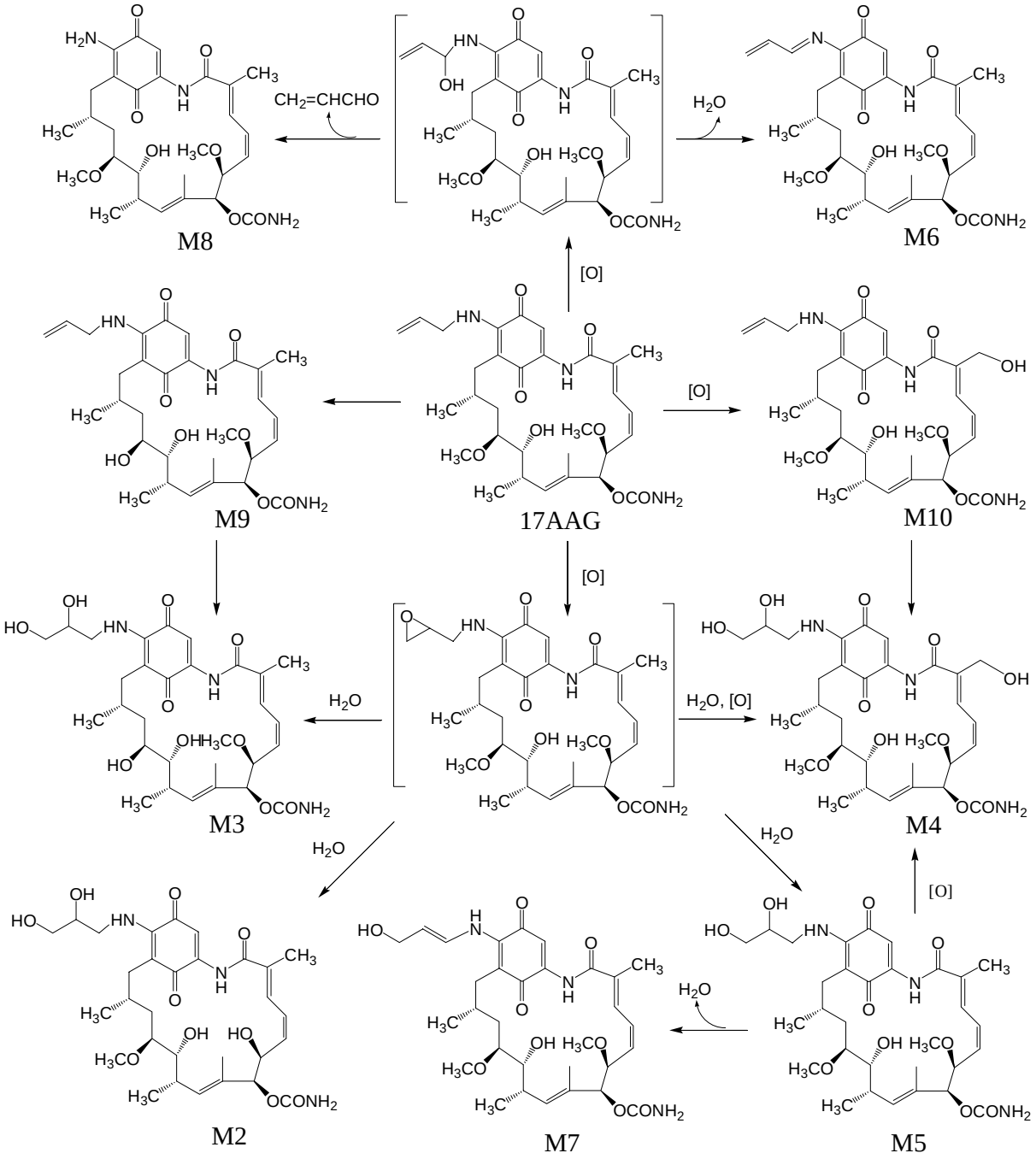

DMD Fast Forward. Published on September 29, 2006 as DOI: 10.1124/dmd.106.009639
This article has not been copyedited and formatted. The final version may differ from this version.

Fig. 6